A Unifying Theory of Driver Perception and Steering Control on Straight and Winding Roads

El, Kasper van der; Pool, Daan M.; van Paassen, Marinus Rene M.; Mulder, Max

DOI
10.1109/THMS.2019.2947551

Publication date
2019

Document Version
Accepted author manuscript

Published in
IEEE Transactions on Human-Machine Systems

Citation (APA)
El, K. V. D., Pool, D. M., van Paassen, M. R. M., & Mulder, M. (2019). A Unifying Theory of Driver Perception and Steering Control on Straight and Winding Roads. *IEEE Transactions on Human-Machine Systems*, *50*(2), 165-175. Article 8890716. Advance online publication. https://doi.org/10.1109/THMS.2019.2947551

A Unifying Theory of Driver Perception and Steering Control on Straight and Winding Roads

Kasper van der El, *Member, IEEE*, Daan M. Pool, *Member, IEEE*, Marinus René M. van Paassen, *Senior Member, IEEE*, and Max Mulder, *Member, IEEE*

***Abstract*—Novel driver support systems potentially enhance road safety by cooperating with the human driver. To optimize the design of emerging steering support systems, a profound understanding of driver steering behavior is required. This article proposes a new theory of driver steering, which unifies visual perception and control models. The theory is derived directly from measured steering data, without any *a priori* assumptions on driver inputs or control dynamics. Results of a human-in-the-loop simulator experiment are presented, in which drivers tracked the centerline of straight and winding roads. Multiloop frequency response function (FRF) estimates reveal how drivers use visual preview, lateral position feedback, and heading feedback for control. Classical control theory is used to model all three FRF estimates. The model has physically interpretable parameters, which indicate that drivers minimize the bearing angle to an "aim point" (located 0.25–0.75 s ahead) through simple compensatory control, both on straight and winding roads. The resulting unifying perception and control theory provides a new tool for rationalizing driver steering behavior, and for optimizing modern steering support systems.**

***Index Terms*—Driver steering, multiloop control, preview information, system identification, visual perception.**

I. Introduction

ROAD vehicles are rapidly being equipped with driver assistance systems and autopilots for temporary automatic control. Human-like and individualized automatic controllers may prove key to optimize the cooperation between the driver and an automation system [1], [2], but designing such systems requires a profound understanding of human driver behavior.

Considering *steering* on winding roads, the driver's primary task is to keep the vehicle between the two lane edges. Steering in essence comprises two processes: 1) selection of perceptual feedbacks (the driver *inputs*), and 2) processing of the selected feedbacks into a steering output (the driver *control dynamics*). While drivers are known to rely strongly on visual feedback [3]–[5], over five decades of research has not led to a widely accepted theory that unifies both driver visual perception and steering control.

Manuscript received February 3, 2019; revised July 27, 2019; accepted September 22, 2019. This article was recommended by Associate Editor N. A. Stanton. *(Corresponding author: Kasper van der El.)*

The authors are with the Control and Simulation Section, Faculty of Aerospace Engineering, Delft University of Technology, 2629 HS Delft, The Netherlands (e-mail: k.vanderel@tudelft.nl; d.m.pool@tudelft.nl; m.m.vanpaassen@tudelft.nl; m.mulder@tudelft.nl).

Color versions of one or more of the figures in this article are available online at http://ieeexplore.ieee.org.

Digital Object Identifier 10.1109/THMS.2019.2947551

In fact, two scientific approaches have emerged, each of which focuses on one of the two steering processes [6], [7]. The *information-centered* approach predominantly studies the visual cues used by drivers. Using experimental tools such as eye-trackers and visual occlusion, evidence has been provided that drivers rely on patterns of the optical flow [3], [4], [8]–[10], both "near" and "far" visual regions [10]–[13], and the road's curvature or tangent point [14]–[16]. In contrast, the *control-theoretic* approach mostly ignores driver perception and focuses on understanding and modeling the driver's control dynamics. Control theory has clarified that drivers combine feedforward (preview) control to anticipate on the road's upcoming curves, with stabilizing feedback control to suppress disturbances such as wind gusts [17]–[21].

To accurately predict how drivers will interact with novel support technologies (e.g., in haptic-shared controllers [1], [2]), it has become clear that a *unifying* theory is needed that resembles both driver visual perception *and* control [6], [7]. For example, the currently popular *two-point models* [22], [23] combine state-of-the-art manual control theory [24], [25] with feedback from near and far bearing angles in the driver's visual field [11]. Unfortunately, such models in general require assumptions on both the driver inputs and control organization, so they fail to explain—and are unsuitable for studying—how drivers *adapt* their perceptual feedbacks and control dynamics to task variables and novel technologies.

There is in fact a direct link between the information-centered and control-theoretic approaches, as visual cues are related to the vehicle outputs by the *perspective geometry* [6]. By first estimating the human's multiloop control dynamics with *system identification* techniques, the perspective geometry has already revealed which visual cues humans use for control in various flying and driving tasks [17], [26]–[28]. For example, Weir and McRuer [17], [26] showed that driver steering on *straight roads* resembles a compensatory control strategy, based on the visual bearing angle to an "aim point" on the road centerline approximately 0.5 s ahead. To similarly estimate the visual cues used for steering on *winding* roads, data of the driver's feedforward, *preview* response dynamics are additionally required. While the preview response dynamics have never been directly measured in driving tasks, they have recently been measured in laboratory tracking tasks using frequency-domain system identification techniques [29], [30]; these techniques may thus also reveal exactly *what parts* of the previewed road drivers use for steering and *how*.

This article aims to provide a new unified theory of driver steering on straight and winding roads, which includes both perception and control. The theory is derived directly from data obtained in a human-in-the-loop simulator experiment, without any *a priori* assumptions about the driver's perceptual feedbacks or control dynamics. To do so, the data are analyzed with a multiloop, instrumental-variable system identification technique, yielding frequency response function (FRF) estimates of *three* driver responses, based on: 1) heading feedback, 2) lateral position feedback, and, most crucially, 3) road preview (feedforward). These estimates facilitate the formulation of a control-theoretic model that accurately captures the driver's *multiloop* steering behavior. Additionally, using the perspective geometry, the model reveals the visual cues used by drivers for control. The obtained model *explains* driver steering and allows for *predicting* effects of different look-ahead times. Preliminary results of the experiment have previously been presented at the 2018 IEEE SMC conference, see [31] for details.

II. Linking Visual Information to Control Theory: Perspective Geometry

The driver's control task is illustrated in Fig. 1. The driver follows a certain target trajectory (e.g., given by the lateral position of the road centerline y_c), by rotating the steering wheel with angle δ. External disturbances (e.g., wind gusts, y_d, and ψ_d) can perturb the vehicle's lateral position y and heading ψ.

Equivalently, drivers minimize the *current* lateral position error $y_e(t) = y_c(t) - y(t)$. However, $y_e(t)$ is located directly below the vehicle, see Fig. 1(c), and is thus not visible from the driver's view through the vehicle's front windscreen. The driver must instead rely on available visual cues to obtain indirect information about $y_e(t)$. Possible perceptual feedbacks include static optical features like the bearing and splay angles of the road edges, and dynamical cues (i.e., the optical flow) such as the *rate of change* of these bearing and splay angles [4], [32], [33]. Control-theoretic models typically ignore driver feedback selection; for example, see Weir and McRuer [17], [26], Donges [18], and MacAdam [34]. These models directly use the tracking error, the vehicle states, or the previewed road as inputs, which is illustrated in Fig. 1(b).

The *perspective geometry* provides a mathematical relation between the optical cues and the vehicle states. Fig. 1(a) shows a single perceptual variable: the bearing angle η to an "aim point" on the road T_{la} s ahead of the vehicle. Using Fig. 1(c), the bearing angle η can be expressed as function of the vehicle and aim-point lateral positions y and $y_c^\star$, and the vehicle heading ψ, as follows:

$$\begin{aligned}\eta(t+T_{la}) &= \psi_c^\star(t+T_{la}) - \psi(t)\\ &= \arcsin\left(\frac{y_c^\star(t+T_{la}) - y(t)}{D}\right) - \psi(t)\\ &\approx \frac{y_c^\star(t+T_{la}) - y(t)}{U_0 T_{la}} - \psi(t), \qquad \text{for small } \psi.\end{aligned} \tag{1}$$

All symbols are defined in Fig. 1(c). Equation (1) is important, because it shows that a response to the optical bearing angle is

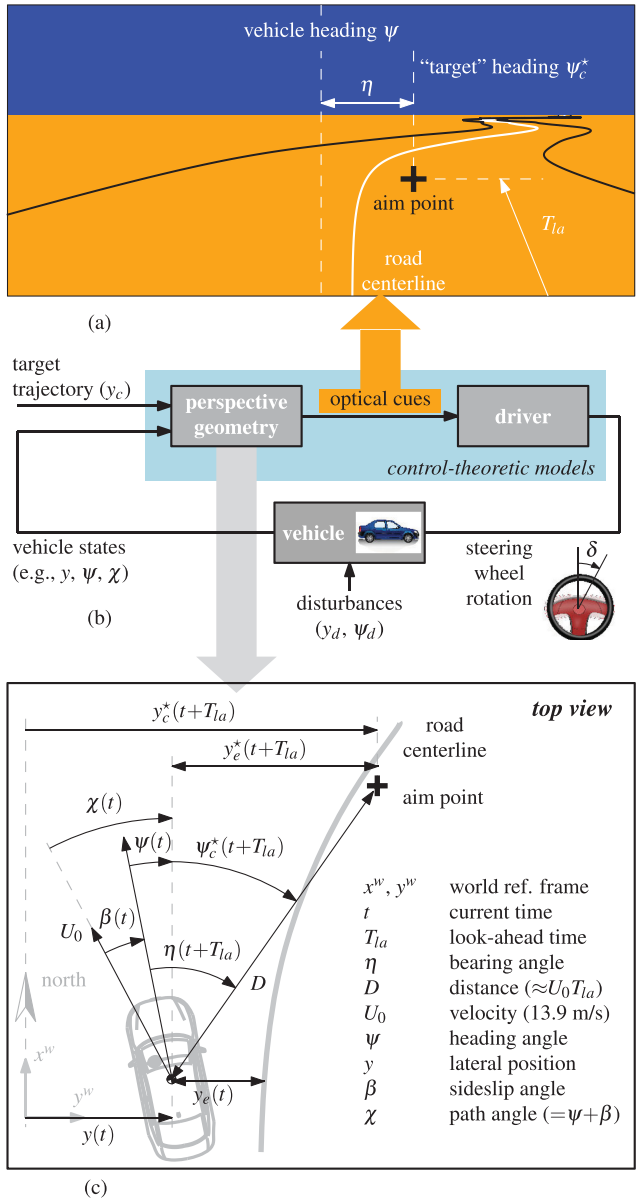

Fig. 1. Illustration of the driver's perspective view on a winding road (a), with the bearing angle η to an "aim point" indicated in white. Schematic of the driver in a steering task (b), with the scope of typical control-theoretic models in blue, lumping the perspective geometry and driver blocks and ignoring driver visual cue selection. The top view on the winding road (c) reveals the geometric relation between the optical cue η on the one hand, and the vehicle states (y and ψ) and the aim point ($y_c^\star$) on the other hand.

equivalent, from a control-theoretic perspective, to *three* driver control responses with respect to $y_c^\star(t+T_{la})$, $y(t)$, and $\psi(t)$. Moreover, these three control-theoretic responses *are not independent*: lateral position and heading feedback are relatively *weighed* by a factor $\frac{1}{U_0 T_{la}}$ that depends on the look-ahead time T_{la}, while the same T_{la} appears as a *time shift* in the aim point lateral position $y_c^\star(t+T_{la})$. As will become clear later, this "match" of T_{la} is key to this article. Expressions similar to (1) can be derived for other optical cues (e.g., see [6] for details), but are not further investigated here, as various researchers have suggested that the bearing angle is a key perceptual feedback

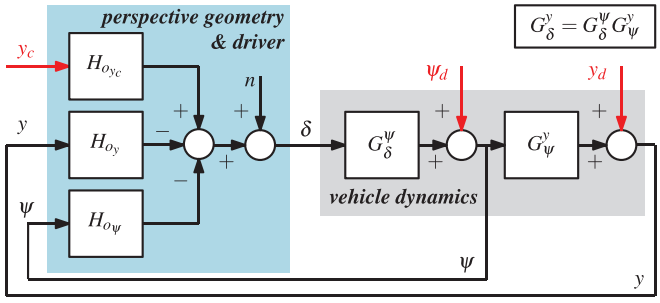

Fig. 2. Closed-loop control diagram used for measuring the driver's multiloop response properties (lumped together with the perspective geometry). The three external forcing functions are indicated in red.

that guides driver steering [26], [33]. Possible bearing angle aim-points are the tangent point, points on the road's lane edge or centerline, or points on the future vehicle path [2], [10], [22], [33], [35].

III. Method

This article tests the hypothesis that drivers respond to an aim-point bearing angle. To do so, experimental human-in-the-loop data are analyzed with system identification techniques.

A. System Identification Approach

Fig. 2 shows the lumped combination of the perspective geometry and the driver as a three-channel controller in the quasi-linear framework [24]. The three linear responses are 1) a *feedback* H_{o_ψ} to vehicle heading, 2) a *feedback* H_{o_y} to vehicle lateral position, and 3) a *feedforward* $H_{o_{y_c}}$ to the lateral position of the previewed road centerline. Remaining nonlinearities, time-varying behavior, and injected noise are accounted for by the remnant $n(t)$. This three-channel organization provides a convenient tool for estimating the driver's multiloop response properties, and hence for verifying whether or not drivers use an aim-point bearing angle as perceptual feedback. Nonetheless, it is not assumed that drivers are organized as the three-channel controller in Fig. 2, or even close these particular control loops. All other vehicle states (e.g., $\chi, \beta, \dot{\psi}$) and tracking errors (y_e, ψ_e) are a (linear) combination of the y_c, y, and ψ inputs, see Fig. 1(c), so responses to these signals are indirectly also captured by measuring $H_{o_{y_c}}$, H_{o_y}, and H_{o_ψ}.

1) FRF Estimation: With an instrumental-variable, frequency-domain system identification technique, FRFs of $H_{o_{y_c}}$, H_{o_y}, and H_{o_ψ} can be estimated without making *a priori* assumptions about their dynamics [36]. Three instrumental variables are required to disentangle the three responses. Therefore, three external *forcing functions* are applied in the experiment, see Fig. 2: the road y_c, and two disturbances y_d and ψ_d, which appear to the driver as side-wind gusts that perturb the vehicle lateral position and heading, respectively. The use of random-appearing multisine signals, with mutually exclusive sets of input frequencies $\omega_{y_c}, \omega_{\psi_d}$, and ω_{y_d}, guarantees that the forcing functions are uncorrelated and can serve as instrumental variables [36]. Using Fig. 2, the Fourier transform of the control output can be written as:

$$\delta(j\omega) = H_{o_{y_c}}(j\omega)Y_c(j\omega) - H_{o_\psi}(j\omega)\psi(j\omega) - H_{o_y}(j\omega)Y(j\omega) + N(j\omega). \quad (2)$$

To solve for $H_{o_{y_c}}(j\omega)$, $H_{o_\psi}(j\omega)$, and $H_{o_y}(j\omega)$, three equations are required. First, (2) is evaluated only at the target signal input frequencies ω_{y_c}. A second equation is obtained by interpolating the measured signals (U, Y_c, ψ, Y) in the frequency domain from the heading disturbance input frequencies ω_{ψ_d} to these same ω_{y_c} (denoted by $\tilde{U}, \tilde{Y_c}, \tilde{\psi}, \tilde{Y}$). A third equation is obtained similarly, by interpolating from ω_{y_d} to ω_{y_c} (denoted by $\check{U}, \check{Y_c}, \check{\psi}, \check{Y}$). As the remnant $N(j\omega)$ is negligibly small compared to the linear output at the input frequencies [36], the following system of equations is obtained:

$$\begin{bmatrix} U(j\omega_{y_c}) \\ \tilde{U}(j\omega_{y_c}) \\ \check{U}(j\omega_{y_c}) \end{bmatrix} = \begin{bmatrix} Y_c(j\omega_{y_c}) & -\psi(j\omega_{y_c}) & -Y(j\omega_{y_c}) \\ \tilde{Y_c}(j\omega_{y_c}) & -\tilde{\psi}(j\omega_{y_c}) & -\tilde{Y}(j\omega_{y_c}) \\ \check{Y_c}(j\omega_{y_c}) & -\check{\psi}(j\omega_{y_c}) & -\check{Y}(j\omega_{y_c}) \end{bmatrix} \times \begin{bmatrix} H_{o_{y_c}}(j\omega_{y_c}) \\ H_{o_\psi}(j\omega_{y_c}) \\ H_{o_y}(j\omega_{y_c}) \end{bmatrix} \quad (3)$$

which can be solved for $H_{o_{y_c}}(j\omega_{y_c})$, $H_{o_\psi}(j\omega_{y_c})$, and $H_{o_y}(j\omega_{y_c})$ at the frequencies ω_{y_c}. After interpolating all signals to ω_{ψ_d} and ω_{y_d}, (3) similarly provides FRF estimates at those frequencies. Examples of this technique's success in estimating multiloop human control dynamics can be found, amongst others, in [29], [30], and [36].

2) Model Fitting: As the estimated FRFs reveal the driver response dynamics, they directly allow for formulating a control-theoretic model that captures all three steering responses. After proposing a model, it is fit to the data by minimizing the following least-squares criterion:

$$\hat{\Theta} = \underset{\Theta}{\operatorname{argmin}} \sum_{i=1}^{N} |\mathcal{E}(j\omega_i|\Theta)|^2 \quad (4)$$

$$\mathcal{E}(j\omega|\Theta) = \delta(j\omega) - \hat{\delta}(j\omega|\Theta) \quad (5)$$

with $\mathcal{E}(j\omega_i|\Theta)$ the modeling error at a single frequency ω_i and N the total number of input frequencies of the three forcing functions combined. $\delta(j\omega)$ and $\hat{\delta}(j\omega|\Theta)$ are the measured and modeled steering wheel rotations; the latter depends on the model parameter vector Θ, and is obtained by substituting the modeled $H_{o_{y_c}}(j\omega|\Theta)$, $H_{o_y}(j\omega|\Theta)$, and $H_{o_\psi}(j\omega|\Theta)$ into (2) (with remnant $N(j\omega)= 0$). The variance accounted for (VAF) is used as a measure for the model quality-of-fit [29]: VAF $= [1 - (\sigma_\epsilon^2/\sigma_\delta^2)] \times 100\%$, with σ_ϵ^2 the variance of the modeling error in (5), and σ_δ^2 the variance of the measured control output.

B. Driving Experiment

1) Driving Task and Apparatus: The experimental setup is shown in Fig. 3. An abstract world scenery was presented which showed only the road centerline, in order to limit variability in participants' steering behavior, and no physical motion feedback was provided. Participants were instructed to follow the

Fig. 3. Picture of the experimental setup during the experiment, inside the SIMONA research simulator (SRS) of TU Delft. This simulator is often used for aviation research, but was adapted to driving for the current experiment.

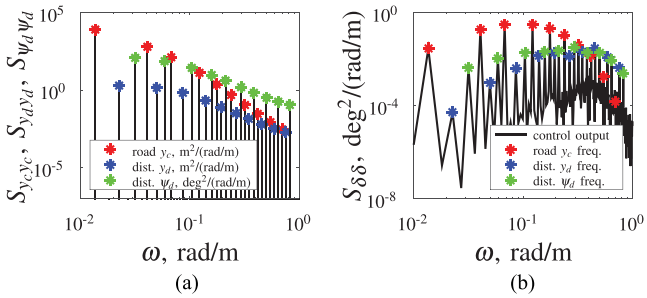

Fig. 4. Power spectra of the three experimental forcing functions (a), and the measured control-output spectrum of Participant 1, averaged over the five measurement runs (b).

road centerline as accurately as possible (a *tracking* task). The centerline was 10 cm wide and was viewed from 1 m height. Visuals were presented on the simulator's collimated projection system, which provided a 180×40 deg field of view. The vehicle moved at constant forward velocity $U_0 = 50$ km/h. The inner- (ψ) and outer-loop (y) vehicle dynamics, $G^{\psi}_{\delta}(j\omega) = \frac{1.33}{j\omega}$ and $G^{y}_{\psi}(j\omega) = \frac{U_0}{j\omega}$ in Fig. 2, were pure integrators, identical as used by Donges [18] and Land and Horwood [11]. The simulator's left-hand side was equipped with a customized, electrically-driven passenger-car steering wheel. The steering wheel stiffness was set to 0.087 Nm/deg within 5.7 deg of the neutral position and to 0.131 Nm/deg otherwise, the damping ratio was 0.007 Nm· s/deg and inertia was 0.2 kg· m^2. Steering wheel rotations were limited to $\pm$45 deg due to hardware limitations.

Participants performed four tasks: driving on straight (S, $y_c = 0$) or winding roads (W, $y_c \neq 0$), each with rotational visual feedback (tasks 1 and 2) and without (tasks 3 and 4). This article presents only the results of the *natural* straight and winding road driving tasks *with* rotational feedback; results of the other two tasks can be found in [31].

2) Road Trajectory and Disturbances: The road centerline and disturbance signals were designed to be the sum of ten sinusoids; for example, the centerline trajectory is given by

$$y_c(a) = \sum_{k=1}^{10} A_{y_c}[k] \sin(\omega_{y_c}[k]a + \phi_{y_c}[k]) \tag{6}$$

with amplitude $A_{y_c}[k]$, frequency $\omega_{y_c}[k]$, and phase $\phi_{y_c}[k]$ of the kth sinusoid, and a the along-track distance [37]. The longitudinal centerline coordinates are $x_c(a) = \int \cos(\psi_c(a))da$, with the road heading given by $\psi_c(a) = \arcsin(\frac{dy_c}{da})$. The heading and lateral position disturbances $y_d(a)$ and $\psi_d(a)$ were defined identical to (6), and were applied directly in the vehicle body reference frame. All forcing function parameters can be found in [31]. To avoid spectral leakage, all frequencies $\omega[k]$ were selected to be integer multiples of the fundamental measurement frequency ($\frac{2\pi}{1389} = 0.0045$ rad/m), with 1389 m the centerline track length. The total track length driven by participants per measurement run was 1806 m; the first 278 m (run-in) and last 139 m (run-out) were not analyzed. The forcing function amplitudes $A[k]$ were scaled to obtain a realistic driving task, see Fig. 4(a) for their spectra. An example of measured control outputs is shown in Fig. 4(b), to illustrate that participants steered predominantly at the forcing function input frequencies (the peaks in the spectrum), and above all at the centerline frequencies ω_{y_c}, so the task predominantly involved *road following*.

3) Participants and Procedures: Eight motivated volunteers participated in the experiment, all students or staff from TU Delft. Participants signed for informed consent prior to the experiment. First, a single run of each condition was performed to familiarize participants with the steering wheel, the vehicle dynamics, and the display. Then, the four experimental conditions were performed in an order randomized over sets of four participants according to a balanced Latin-square design. A condition was performed at least until tracking performance (rms(y_e)) and control activity (rms(δ)) were approximately constant in five consecutive runs, which were then used for analysis. The applied steering wheel rotations $\delta(t)$ and the vehicle lateral position $y(t)$ and heading $\psi(t)$ were recorded at 100 Hz.

4) Data Analysis: The collected data were interpolated offline to constant along-track distance intervals $\Delta a = 0.1389$ m, to facilitate the frequency-domain analysis without leakage. All signals were averaged over the five measurement runs in the frequency domain to reduce effects of remnant noise on the FRF and model parameter estimates. Final results are presented as function of the temporal frequency (i.e., in rad/s), which is obtained by multiplying the spatial, along-track distance frequency (in rad/s) with the forward velocity U_0. This facilitates comparisons with manual control data in the literature (e.g., [17], [26], and [29]), and is a good approximation, as participants completed the 1389 m measurement part of the track always well within 0.5% of the nominal time (100.05 s, the time required to exactly follow the centerline).

IV. Identification and Modeling Results

A. Multiloop FRF Estimates

Fig. 5 shows Bode plots of estimated driver heading, lateral position, and preview response dynamics. No preview response dynamics were estimated in straight road tasks, as $y_c = 0$. The cross markers in Fig. 5 indicate the FRF estimates.

1) Heading Response Dynamics: Fig. 5(a) shows that the $H_{o_\psi}(j\omega)$ FRF estimates approximate gain dynamics at low frequencies and differentiator dynamics at higher frequencies, both in straight and winding road tasks. This can be interpreted

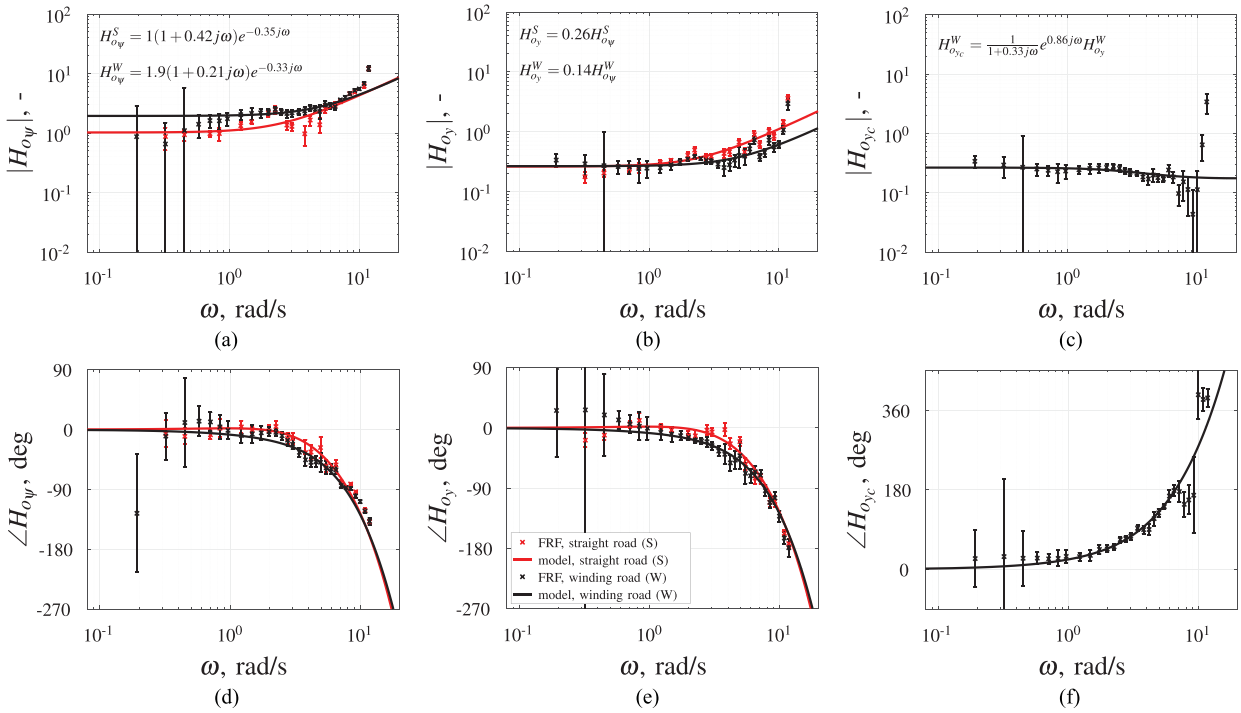

Fig. 5. Bode plots of the estimated multiloop response dynamics for participant 1; FRF estimates with standard errors and model fits. (a) Heading, magnitude. (b) Lateral position, magnitude. (c) Target, magnitude. (d) Heading, phase. (e) Lateral position, phase. (f) Target, phase.

as responses proportional to the vehicle's heading *angle* and *rate*. Furthermore, notable phase lag is visible in Fig. 5(d), with a characteristic roll-off at higher frequencies that reflects the driver's response *time delay*. No evidence of the driver's neuromuscular system dynamics is visible in Fig. 5(a) and (d), suggesting that the neuromuscular bandwidth was higher than the highest forcing function input frequency (11.5 rad/s).

At low frequencies, the gain $H_{o_\psi}(j\omega)$ dynamics equalize the vehicle yaw dynamics $G^{\psi}_{\delta}(j\omega) = \frac{1.33}{j\omega}$ to integrator open-loop dynamics $H_{o_\psi}(j\omega)G^{\psi}_{\delta}(j\omega)$, in agreement with the crossover-model theory [24]. Consequently, the driver's heading response dynamics can be modeled as a compensatory control response, identical to McRuer's simplified precision model [24]

$$H_{o_\psi}(j\omega) = H^{cmp}_{o}(j\omega) = K_{e^\star}(1+T_{L,e^\star}j\omega)e^{-\tau_{e^\star}j\omega} \qquad (7)$$

with gain $K_{e^\star}$, lead time-constant $T_{L,e^\star}$, and time delay $\tau_{e^\star}$.

2) Lateral Position Response Dynamics: Fig. 5(b) and (e) shows that the $H_{o_y}(j\omega)$ FRF estimates have a shape that is identical to $H_{o_\psi}(j\omega)$, approximating gain and differentiator dynamics at low and high frequencies, respectively. However, the magnitude of $H_{o_y}(j\omega)$ is substantially lower than that of $H_{o_\psi}(j\omega)$, so the following model is proposed:

$$H_{o_y}(j\omega) = K^{\psi}_{y}H^{cmp}_{o}(j\omega) \qquad (8)$$

with $H^{cmp}_{o}(j\omega)$ defined by (7) and K^{ψ}_{y} the driver's weighing of heading and lateral position feedback. The observed lateral position and heading feedback dynamics combined, modeled by (7) and (8), are consistent with general theories of multiloop manual control [24], [38]: humans close the inner loop (heading) with dynamics that equalize the open-loop dynamics to an integrator, such that the outer loop (lateral position) can be closed with straightforward proportional control (gain K^{ψ}_{y}).

3) Preview Response Dynamics: In winding road tasks, drivers additionally mechanize the feedforward preview response $H_{o_{y_c}}(j\omega)$. The magnitude of the $H_{o_{y_c}}(j\omega)$ FRF estimates in Fig. 5(c) approximates gain dynamics at low frequencies, while the reduced magnitude at higher frequencies points to integrator dynamics. This suggests that drivers adopt responses proportional to the centerline *lateral position* and *smoothed* lateral position. Note that the FRF estimates at the highest frequencies are unreliable, because the measured control output disappears in the noise, see Fig. 4(b). The phase of the preview response in Fig. 5(f) reveals phase *lead*, which increases towards higher frequencies. This behavior resembles a negative time delay and can be interpreted as a response to the previewed centerline *ahead*.

Comparable preview response dynamics have been measured in single-loop preview tracking tasks (e.g., see [29] and [30]), and were modeled with a target *prefilter* $H_{o_f}(j\omega)$

$$H_{o_{y_c}}(j\omega) = H_{o_f}(j\omega)H_{o_y}(j\omega). \qquad (9)$$

The reason for including the lateral position response model (H_{o_y}) in the preview response dynamics, is that their FRF estimates are near-identical at the lowest frequencies [compare Fig. 5(b) with (c), and (e) with (f)], which suggests that identical (inner-loop) dynamics are visible in both estimates. The following prefilter dynamics are consistent with the estimated FRFs in

Fig. 5, and are identical to the preview model of [29], [30]:

$$H_{o_f}(j\omega) = K_f \frac{1}{1 + T_{l,f} j\omega} e^{\tau_f j\omega} \tag{10}$$

with K_f the scaling gain, $T_{l,f}$ the low-pass (smoothing) filter time-constant,[1] and τ_f the look-ahead time.

B. Control-Theoretic Model

1) Model Synthesis: In contrast with the parallel multiloop organization in Fig. 2, the FRF estimates suggest that drivers are organized as *series* multiloop controller. The heading response is the innermost loop, because its dynamics (H_o^{cmp}) also appear in the lateral position and preview responses, and can thus be moved to the right of the summation point in Fig. 2. Similarly, it follows that lateral position feedback constitutes the middle loop, and preview feedforward the outer loop. Substituting (7)–(9) in (2) yields for the full model

$$\delta(j\omega) = H_o^{cmp}(j\omega) E^\star(j\omega) + N(j\omega) \tag{11}$$

$$E^\star(j\omega) = K_y^\psi \left[H_{o_f}(j\omega) Y_c(j\omega) - Y(j\omega) \right] - \psi(j\omega). \tag{12}$$

The parameter vector, $\Theta = [K_{e^\star}\ T_{L,e^\star}\ \tau_{e^\star}\ K_y^\psi\ K_f\ \tau_f\ T_{l,f}]^T$, has seven parameters. In straight road driving ($y_c = 0$), K_f, τ_f, and $T_{l,f}$ are redundant, yielding a four-parameter model.

2) Model Fits: The dynamics of the fitted model are shown in the Bode plots in Fig. 5, together with the FRF estimates. The FRF estimates of the driver's lateral position, heading, and preview response dynamics are *all* captured well by the model, both in straight and winding road driving tasks. This result is *not trivial*, given that the model was fit by minimizing the error in steering *output*, see (4), and not in each of the estimated multiloop response dynamics separately. There is a small discrepancy between the model and the FRF estimates at the very lowest and highest input frequencies, because, here, several FRF components are poorly estimated (which is clear from the large errorbars in Fig. 5) and possibly also because the driver's neuromuscular system dynamics were not explicitly modeled. The model also closely matches participants' steering *output*, with VAFs that are well above 90% for all eight participants (see Tables I and II).

3) Parameters Estimates: Estimated model parameters, given in Tables I and II, are comparable to values found in other manual control experiments. For example, the response time delay $\tau_{e^\star}$ is between 0.3 and 0.4 s for all participants, while values between 0.25 and 0.6 s are typically reported in the literature [18], [26]. The farthest point of the previewed centerline trajectory that is used for control in winding road tasks, characterized by τ_f, is on average positioned around 0.9 s ahead, comparable to preview tracking tasks [30], and almost identical to the position of the "far point" (0.93 s) measured by Land and Horwood [11] in their visual occlusion driving experiment.

[1] Alternatively, the observed high-frequency smoothing behavior can be modeled by taking the (weighed) average of two viewpoints, much like in recent two-point driver models [2], [22]. However, here, a low-pass filter is chosen because this captures the centerline smoothing behavior with a *single* parameter ($T_{l,f}$) and because the shape of the FRF phase in Fig. 5(f) reflects the behavior of a single negative time delay.

TABLE I
MODEL VAFS AND ESTIMATED PARAMETERS, STRAIGHT ROAD

subj. #	VAF %	$K_{e^\star}$ rad/rad	$T_{L,e^\star}$ s	$\tau_{e^\star}$ s	K_y^ψ rad/m
1	95.24	1.02	0.42	0.35	0.26
2	93.37	1.12	0.40	0.35	0.14
3	95.09	0.76	0.60	0.39	0.17
4	94.65	0.84	0.54	0.37	0.18
5	95.38	1.95	0.23	0.32	0.14
6	94.65	1.44	0.29	0.37	0.15
7	92.20	1.45	0.33	0.32	0.21
8	96.08	0.97	0.43	0.35	0.21

TABLE II
MODEL VAFS AND ESTIMATED PARAMETERS, WINDING ROAD

subj. #	VAF %	$K_{e^\star}$ rad/rad	$T_{L,e^\star}$ s	$\tau_{e^\star}$ s	K_y^ψ rad/m	K_f m/m	τ_f s	$T_{l,f}$ s
1	95.03	1.94	0.21	0.33	0.14	1.00	0.86	0.33
2	93.05	2.22	0.17	0.31	0.10	1.00	0.90	0.19
3	95.15	1.97	0.19	0.35	0.10	1.00	0.84	0.12
4	94.32	1.88	0.20	0.35	0.13	1.00	1.00	0.43
5	95.15	2.27	0.17	0.31	0.13	1.00	0.85	0.29
6	92.13	1.82	0.22	0.37	0.12	1.00	1.05	0.44
7	94.25	2.28	0.19	0.32	0.13	1.00	0.67	0.09
8	94.85	2.07	0.16	0.33	0.10	1.00	0.91	0.21

Tables I and II show that participants generated more lead (higher $T_{L,e^\star}$), and relied relatively less on heading feedback (lower $K_{e^\star}$, higher K_y^ψ) in straight road tasks, as compared to winding road tasks. Table II further shows that the estimate of K_f equals exactly one for all eight participants, so this parameter can be dropped from the model. Consequently, only six parameters are required to capture all characteristic dynamics of driver steering on winding road.

C. From Control Theory to Visual Cues

1) Physical Interpretation of Modeled Behavior: The derived model, given by (11) and (12), suggests that drivers minimize a certain error variable $e^\star$ through compensatory control; the key question then is *which error*. In Section II, it was explained that the perspective geometry connects control theory to visual cues. Comparison of (12), the modeled error $e^\star$, with the Fourier transform of the aim-point bearing angle η in (1), reveals that $e^\star = \eta$ when

$$\text{feedforward:}\quad H_{o_f}(j\omega) Y_c(j\omega) = Y_c^\star(j\omega) e^{T_{la} j\omega} \tag{13}$$

$$\text{feedback:}\quad K_y^\psi = \frac{1}{U_0 T_{la}}. \tag{14}$$

The first equality, (13), essentially states that the preview prefilter $H_{o_f}(j\omega)$ should output a single aim-point T_{la} s ahead. Evaluating the modeled prefilter in the time domain, as done in Fig. 6, yields the *convolution* of the prefilter's impulse response with the previewed trajectory ahead (up to τ_f), which output can indeed be considered as a *single* aim point. The position of the aim point ahead can be approximated by $\tau_f - T_{l,f}$, as

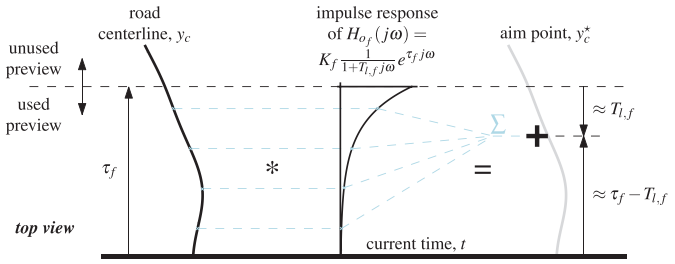

Fig. 6. Modeled centerline filter H_{o_f} can be interpreted as the driver's mapping of the previewed centerline y_c into an aim point $y_c^\star$. Illustrated is the time-domain convolution of the impulse response of H_{o_f} with the centerline up to τ_f s ahead, which can be interpreted as a particular preview weighting by the driver (also see [39]). The position of the resulting aim point ahead can be approximated by $\tau_f - T_{l,f}$, because the phase lag effects of $\frac{1}{1+T_{l,f}j\omega}$ equal those of a pure delay at low frequencies.

explained in Fig. 6, such that the equality in (13) simplifies to $\tau_f - T_{l,f} = T_{la}$.

The second equality, (14), reflects that the control-theoretic model gain K_y^ψ, the driver's relative weighing of lateral position and heading feedback, can also be interpreted as a look-ahead time. "Looking" closer ahead (lower T_{la}) corresponds to a stronger reliance on lateral position feedback (higher K_y^ψ), and *vice versa*.

2) Evidence of Bearing Angle Control on Winding Roads: The crucial point of (13) and (14) is that *together*, they allow for testing whether drivers use the aim-point bearing angle as perceptual feedback in winding road driving tasks. This is the case when $\tau_f - T_{l,f} = \frac{1}{K_y^\psi U_0}$, that is, when the estimated feedback and feedforward responses correspond to *the same look-ahead time*. Fig. 7 shows that, indeed, *all eight* participants tuned their feedback and feedforward control dynamics to correspond to the same look-ahead time. To better appreciate this striking equality, note that from a control-theoretical perspective, the two look-ahead times emerge from two *fully independent* processes.

1) The driver's relative weighing of heading and lateral position *feedback* (K_y^ψ) manifests as the difference in magnitude between the FRF estimates in Fig. 5(a) and (b).
2) The driver's *feedforward*, the processing of the previewed trajectory (H_{o_f}) into an aim point shifted $\tau_f - T_{l,f}$ s ahead, manifests as the characteristic increase in phase towards higher frequencies of the preview response FRF estimates, in Fig. 5(f).

This *confirms* the main hypothesis of this article: drivers use the aim-point bearing angle η as perceptual feedback for steering, as illustrated in Fig. 1(a). Estimated aim-point look-ahead times are between 0.5 and 0.75 s for all participants, as illustrated in Fig. 7(b). Substituting T_{la} for both $\tau_f - T_{l,f}$ and $\frac{1}{K_y^\psi U_0}$ in the model means that *only five parameters* are required to capture the driver's control output, control dynamics, *and* selection of visual feedbacks in winding road tasks. A control diagram of the final model is given in Fig. 8 .

3) Bearing Angle Control on Straight Roads: It is impossible to validate the equality of (13) and (14) in straight road tasks, where drivers lack a preview response. As has been explained

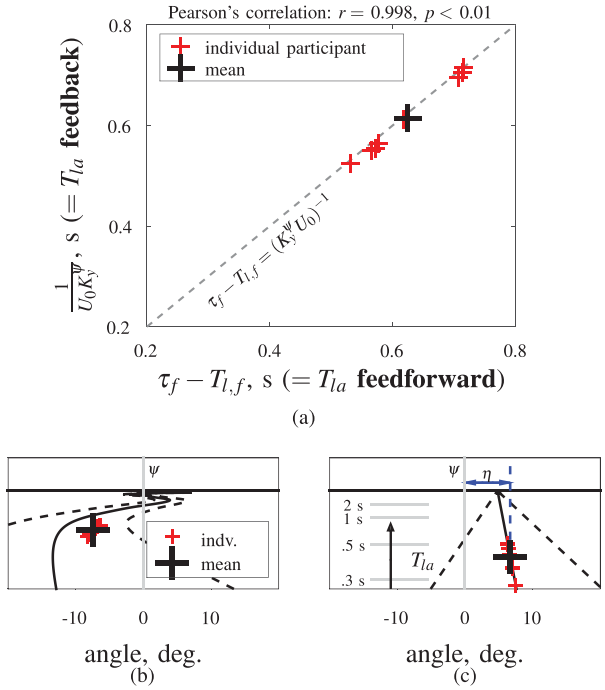

Fig. 7. Correlation between the look-ahead times T_{la} in the control-theoretic feedforward and feedback response channels in the winding road task (a), based on parameters estimates in Table II, and the estimated look-ahead times ($T_{la} = \frac{1}{K_y^\psi U_0}$) for winding (b), and straight road tasks plotted in perspective (c).

in the literature (e.g., [38] and [33]), the driver's weighing of heading and lateral position feedback on straight roads can equally be the result of separate responses to the road's vanishing point (heading information) and splay angle (lateral position information), as by a single aim-point bearing angle response. Nonetheless, assuming that drivers use comparable perception and control strategies on straight and winding roads, it follows that the aim-point bearing angle is also the driver's main perceptual feedback on straight roads. Using (14) to estimate the aim-point look-ahead times in straight road tasks yields values between 0.25 and 0.55 s for the eight participants, see Fig. 7(c). Note that for straight road driving, the exact same aim-point model was previously proposed by Weir and McRuer [17], [26].

V. Model Analysis

With the main hypothesis of this article confirmed, the new unified perception and control model will be used to rationalize and predict (adaptations of) driver steering behavior.

A. Feedforward Control: Preview Prefilter

First, it is investigated *why* equalizing the feedback ($\frac{1}{U_0 K_y^\psi}$) and feedforward ($\tau_f - T_{l,f}$) look-ahead times is a particularly "good" control strategy, not only because it is perceptually convenient, but also from a performance perspective. To do so, the originally proposed seven-parameter model is used.

1) Perfect Target-Tracking Dynamics: Drivers follow a road centerline perfectly when $y_e(t) = 0$, or equivalently, when

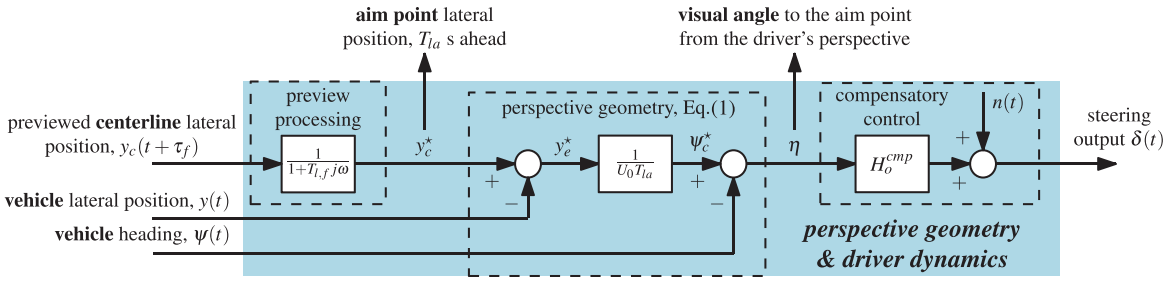

Fig. 8. Driver steering model, which combines visual feedback selection and control, and driving on straight ($y_c = y_c^\star = 0$) and winding roads (full model). The model is consistent with the estimated driver multiloop FRFs in Fig. 5.

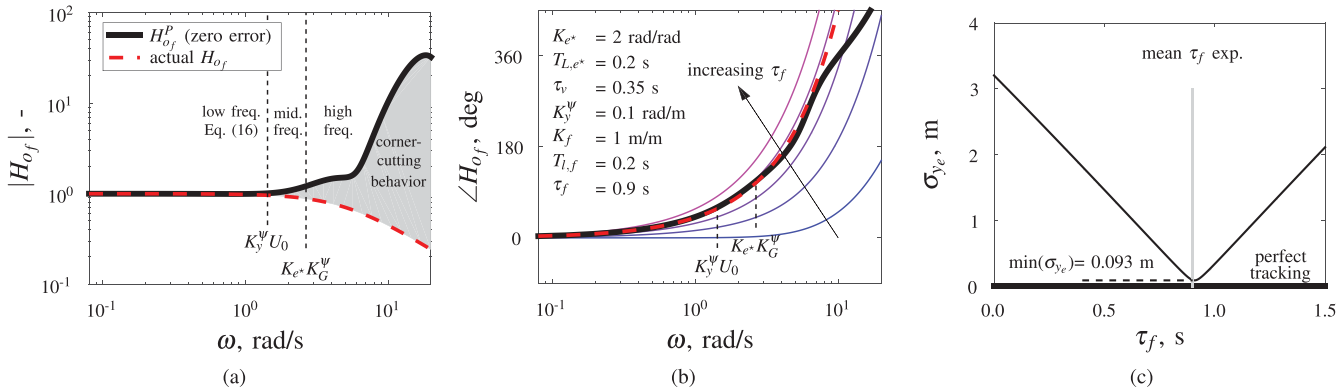

Fig. 9. Bode plots of the preview prefilter dynamics H_{o_f} (a), (b), based on the estimated model parameters in Table II. The time constants $\frac{1}{K_y^\psi U_0}$ and $\frac{1}{K_{e^\star} K_G^\psi}$ follow from (16). The feedforward look-ahead time τ_f markedly affects the standard deviation of the lateral position errors σ_{y_e} (c).

$y(t) = y_c(t)$. From Fig. 2, it follows that the closed-loop dynamics due to y_c (neglecting y_d, ψ_d, and n) are given by

$$\frac{Y(j\omega)}{Y_c(j\omega)} = \frac{G_\delta^y(j\omega) H_{o_{y_c}}(j\omega)}{G_\delta^y(j\omega) H_{o_y}(j\omega) + G_\delta^\psi(j\omega) H_{o_\psi}(j\omega) + 1}. \quad (15)$$

After substituting $Y(j\omega) = Y_c(j\omega)$, together with the modeled driver control dynamics from (7)–(9) and the vehicle dynamics, the following expression can be obtained for the "perfect" prefilter dynamics that yield $y_e(t) = 0$:

$$H_{o_f}^P(j\omega) = \underbrace{1}_{\text{low freq.}} + \underbrace{\frac{1}{K_y^\psi U_0} j\omega}_{\text{middle freq.}} + \underbrace{\frac{1}{K_G^\psi U_0 K_y^\psi H_o^{cmp}} (j\omega)^2}_{\text{high freq.}}. \quad (16)$$

This equation shows that perfect centerline tracking requires a direct unfiltered response to the centerline's lateral position y_c at low frequencies, and responses to the derivative (heading) and second derivative (curvature) at increasingly higher frequencies. Example $H_{o_f}^P(j\omega)$ dynamics are shown in Bode plots in Fig. 9. The strict separation between frequency regions suggested by (16) is not visible in practice, because the three terms partially cancel each other due to phase differences. Fig. 9 reveals that drivers who adopt prefilter dynamics that approximate a gain in magnitude, and a negative delay in phase, can attain near-perfect centerline tracking up to approximately 7 rad/s.

2) Analysis of Measured Prefilter Dynamics: Measured driver prefilter dynamics $H_{o_f}(j\omega)$ match the *phase* required for perfect target-tracking well, see Fig. 9(b). However, the magnitude of the measured $H_{o_f}(j\omega)$ dynamics reveals explicit *lag* behavior (centerline smoothing) at higher frequencies, as opposed to the lead dynamics required for perfect target-tracking, see Fig. 9(a). Together, this indicates that drivers synchronize the vehicle's lateral position movements well with the changes in centerline lateral position, while *cutting corners* at high frequencies.[2] For the data in Fig. 9, the standard deviation of the vehicle's lateral position deviation from the centerline $\sigma_{y_e} \approx 0.1$ m, which is sufficiently low for safe lane keeping on most roads; measured deviations on real roads are typically higher [10], because the current model analysis lacks external disturbances (y_d, ψ_d) and human remnant (n).

3) Optimal Feedforward Look-Ahead Time: The measured driver preview prefiltering dynamics are *suboptimal*, as $\sigma_{y_e} > 0$ m. However, Fig. 9(b) clearly shows that the effective feedforward look-ahead time ($\tau_f - T_{l,f}$) *is* optimal, and that y_e increases sharply when, for example, only τ_f is changed [see Fig. 9(c)]. A τ_f that is just 0.3 s away from the optimum yields a striking *ten-fold* increase in the lateral deviations.

[2]In preview tracking tasks, human controllers occasionally adopt a high-frequency, open-loop response in parallel to the control response observed here. The additional, fast open-loop response allows for matching $H_{o_f}^P$ also at high frequencies and leads to improved target tracking. However, such a high-frequency response comes at the cost of substantial control effort, and appears to be mechanized only by experienced controllers in tasks with high-frequency target signals and first-order (or lower) vehicle dynamics [40], [41].

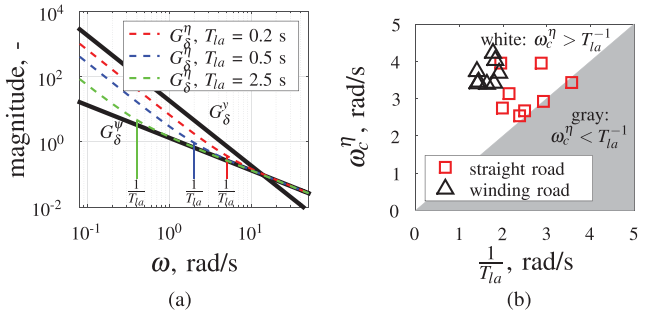

Fig. 10. Bode magnitude plot of the inner- (heading, G_δ^ψ) and outer-loop (lateral position, G_δ^y) vehicle dynamics, and the aim-point bearing angle dynamics $G_\delta^\eta(j\omega, T_{la})$ for three look-ahead times T_{la} (a). Measured bearing angle open-loop crossover frequencies ω_c^η (b), as a function of the measured $1/T_{la}$, the break frequency of $G_\delta^\eta(j\omega, T_{la})$.

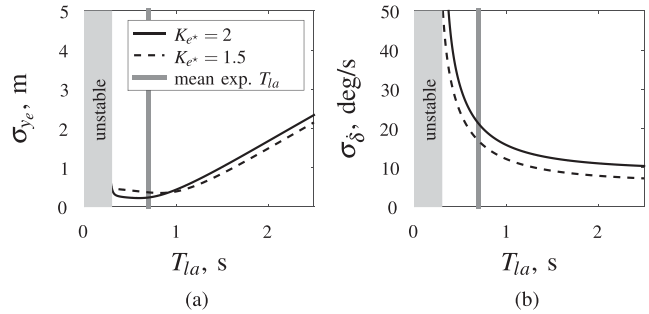

Fig. 11. Simulated effects of the look-ahead time T_{la} on tracking performance σ_{y_e} (a) and control activity $\sigma_{\dot\delta}$ (b). Other model parameters are fixed at the values shown in Fig. 9. The vertical gray line indicates the average experimental T_{la} estimate (the average experimental $K_{e^\star} \approx 2$ rad/rad).

From the perfect target-tracking dynamics in (16), an expression can be derived for the optimal feedforward look-ahead time. The best match with the phase of $H_{o_f}^P(j\omega)$ at low and middle frequencies is obtained when the effective feedforward look-ahead time $\tau_f - T_{l,f}$ of the driver's prefilter H_{o_f} approximates the highest time constant in (16), which, remarkably, is $\frac{1}{K_y^\psi U_0}$. This is the exact same equality that indicated a response to the aim-point bearing angle, and was shown to be perfectly satisfied by all eight participants, see Fig. 7. The severe performance penalty for poorly tuned look-ahead times explains why bearing angle control is not only perceptually feasible, but also desirable for performance. It explains the near-perfect statistical correlation between $\tau_f - T_{l,f}$ and $\frac{1}{K_y^\psi U_0}$ in Fig. 7.

B. Aim-Point Dynamics and Look-Ahead Time

After dropping K_f and substitution of T_{la}, the model in Fig. 8 was obtained, which reflects that drivers adopt a compensatory control strategy, with the aim-point bearing angle η as error-feedback variable. The driver's selection of an aim-point and the driver's response dynamics therefore *together* determine the attained driving performance and stability.

1) Aim-Point Dynamics: As drivers do not respond directly to the vehicle outputs (e.g., y, ψ), but to the selected visual feedbacks, the *apparent* control task as perceived by the driver is defined by the visual cue dynamics, and not the vehicle dynamics [6], [27]. Visual cue dynamics are the combination of the vehicle dynamics and the perspective geometry, and characterize the movement of the considered visual cue *within the driver's visual field* due to steering inputs. The dynamics of the aim-point bearing angle η are obtained by dividing the Fourier transform of (1) by $\delta(j\omega)$, yielding

$$G_\delta^\eta(j\omega, T_{la}) = \frac{\eta(j\omega)}{\delta(j\omega)} = \frac{-G_\delta^y(j\omega)}{U_0 T_{la}} - G_\delta^\psi(j\omega). \qquad (17)$$

The aim-point dynamics thus depend explicitly on the look-ahead time T_{la} selected by the driver. Fig. 10(a) shows a Bode magnitude plot of the aim-point dynamics for various look-ahead times. $G_\delta^\eta(j\omega, T_{la})$ resembles the vehicle's lateral position dynamics (here, a double integrator) at low frequencies, and the vehicle's heading dynamics (here, a single integrator) at high frequencies. By substituting the vehicle dynamics into (17), it follows that the break frequency is $1/T_{la}$ rad/s.

Selecting an aim point close ahead thus predominantly yields a *double integrator* control task, and requires explicit lead equalization from the driver in $H_o^{cmp}(j\omega)$, according to the crossover model [24]. An aim point far ahead, on the contrary, effectively yields a *single integrator* control task, in which proportional compensatory control suffices. For the performed experiment, Fig. 10(b) shows that the measured crossover frequencies ω_c^η of the open-loop dynamics $G_\delta^\eta(j\omega, T_{la})H_o^{cmp}(j\omega)$ are in general higher than $1/T_{la}$ rad/s. This indicates that crossover occurs at a frequency where the bearing angle open-loop resembles integrator dynamics.

2) Aim-Point Look-Ahead Time: The effects of varying the aim-point look-ahead time T_{la} are also investigated in closed-loop model simulations, identical to those for τ_f variations in Fig. 9. Here, however, the final five-parameter bearing-angle model is used, and the experimental disturbances y_d and ψ_d are additionally included. All model parameters (except T_{la}) are fixed at the values listed in Fig. 9(b).

Fig. 11 shows that the driver-vehicle system becomes unstable when the look-ahead time T_{la} is reduced to below approximately 0.3 s, which is a direct consequence of the bearing angle dynamics that converge to a double integrator and become less stable [see Fig. 10(a)]. Increasing the look-ahead time T_{la} beyond the optimal value (0.5–1 s ahead) in general leads to larger deviations from the centerline [σ_{y_e}, Fig. 11(a)]. A larger look-ahead time further yields smoother control outputs [lower $\sigma_{\dot\delta}$, Fig. 11(b)], while more aggressive steering corrections are predicted for smaller look-ahead times. These model predictions correspond to the behavioral trends measured by Land and Horwood [11] for different look-ahead times in their visual occlusion driving experiment.

Fig. 11 also illustrates the interaction between the driver's two key processes (feedback selection and control). When a compensatory control strategy with a lower response gain $K_{e^\star}$ is adopted (dotted lines in Fig. 11), a higher look-ahead time T_{la} is required to achieve optimal performance, as the minimum in σ_{y_e} in Fig. 11(a) moves to the right. Equivalently, drivers that select an aim point farther ahead (higher T_{la}) should in general

minimize the bearing angle with a lower response gain $K_{e^\star}$ to achieve optimal performance.

VI. Discussion

This article presented a new, unifying theory of driver perception and steering control through an empirical, data-driven approach. Based on steering data, collected in a human-in-the-loop simulator experiment with three uncorrelated forcing functions, *multiloop* FRF measurements of drivers' steering dynamics were obtained. These FRF estimates, in particular of the driver's preview, feedforward response in winding road tasks, provided strong evidence that the visual bearing angle between the vehicle heading and an aim point ahead is the main perceptual feedback that guides steering. Moreover, the FRF estimates showed that the bearing angle is minimized through straight and simple *compensatory control*.

The resulting unifying theory of driver perception and control applies to steering on both straight and winding roads. Drivers select an aim point on the centerline ahead on straight roads [17], [26], while the aim point on winding roads is obtained by smoothing a portion of the centerline ahead. Because the resulting bearing-angle error is minimized through a compensatory control strategy, a unifying framework emerges for manual control behavior that spans tasks as different as compensatory display tracking and steering on winding roads. The derived driver model directly extends the widely-accepted *crossover model theory* [24] for compensatory tracking, and shows that the key difference is *which error* is being minimized by the human controller.

The driver's main, low-frequency control response can be characterized by only two processes: first, selection of an aim point in the visual scene at a look-ahead time T_{la} ahead of the vehicle, and second, minimization of the visual bearing angle between the vehicle heading and the aim point through proportional control (gain $K_{e^\star}$) with a response time delay $\tau_{e^\star}$. Such compensatory control based on a *future* target point is also known as *prospective* control [7], [42]. Additional research is required to establish the range of driving velocities, vehicle dynamics, road widths, and geometries, for which a simple bearing-angle minimization strategy is adequate. Driver lead generation ($T_{L,e^\star}$) and centerline smoothing ($T_{l,f}$) are *auxiliary* high-frequency behaviors, at least for the task performed here, and help to improve on performance, stability, and control effort objectives.

In theory, the baseline, low-frequency control strategy requires visibility of *only* an aim point. This is consistent with the seminal experiment of Land and Horwood [11], in which drivers could follow a road adequately at low driving velocities (i.e., low-frequency control) when only a single one-deg vertical portion of the visual field was available. For accurate steering at higher velocities (comparable to the driving task performed here, with higher frequencies in the forcing functions), Land and Horwood [11] showed that multiple portions of the visual field are required (i.e., "near" and "far" points). Indeed, for the measured high-frequency lead behavior ($T_{L,e^\star}$), drivers may need feedback of the global optical flow to obtain heading rate information [8], [38]. Moreover, for smoothing the centerline's higher frequency oscillations, visual preview of a substantial *portion* of that centerline seems essential [30]. To truly connect the steering behavior measured here with the literature, results of a visual occlusion experiment (e.g., Land and Horwood [11]) should be analyzed with the system identification techniques from this article.

The proposed unified perception and control theory provides a potentially crucial new analytic tool for researchers and engineers. For the first time, it is possible to quantitatively predict the effects of different perceptual feedback selection strategies, which determine closed-loop performance and stability *together* with the driver's control dynamics. The model furthermore allows for predicting exactly *how much preview drivers need* (model parameter τ_f or $T_{la} + T_{l,f}$), and how this depends on the given driving task, such as the driving velocity, vehicle dynamics, and road width and curvature. With proper extensions, the model may be used in future work for quantifying effects of other sensory feedbacks, to assess the fidelity of physical motion feedback provided in driving simulators, or the effects of novel steering support systems with haptic interfaces [1], [2].

VII. Conclusion

This article studied driver steering behavior by measuring and modeling the driver's multiloop response properties. FRF estimates revealed how drivers use visual preview of the road ahead for control, and facilitated the formulation of the first data-driven classical control model that unifies driver perception and control. Perspective geometrical relations suggest that drivers are organized as series controllers. Both on straight and winding roads, drivers minimize the bearing angle to an "aim point" (located 0.25–0.75 s ahead) through compensatory control. Such bearing angle control yields adequate, yet suboptimal centerline-tracking performance, as well as corner-cutting behavior. Extending previous models such as the seminal crossover model, a single framework is now available for analyzing manual control behavior in tasks that range from single-loop compensatory tracking to driver steering on straight and winding roads. The proposed model provides a tool for predicting adaptations in driver control dynamics and, for the first time, also in driver visual feedback selection. The model can thereby be instrumental for rationalizing between-driver variability and for optimizing the design of human-like or individualized steering support systems in modern road vehicles.

References

[1] D. A. Abbink, M. Mulder, and E. R. Boer, "Haptic shared control: Smoothly shifting control authority?" *Cognition, Technol. Work*, vol. 14, no. 1, pp. 19–28, Mar. 2012.

[2] L. Saleh, P. Chevrel, F. Claveau, J. F. Lafay, and F. Mars, "Shared steering control between a driver and an automation: Stability in the presence of driver behavior uncertainty," *IEEE Trans. Intell. Transp. Syst.*, vol. 14, no. 2, pp. 974–983, Jun. 2013.

[3] J. J. Gibson and L. E. Crooks, "A theoretical field-analysis of automobile-driving," *Amer. J. Psychol.*, vol. 51, no. 3, pp. 453–471, 1938.

[4] D. A. Gordon, "Perceptual basis of vehicular guidance: IV," *Public Roads*, vol. 34, no. 3, pp. 53–68, 1966.

[5] M. Sivak, "The information that drivers use: Is it indeed 90% visual?" *Perception*, vol. 25, no. 9, pp. 1081–1089, 1996.

[6] M. Mulder, M. M. van Paassen, and E. R. Boer, "Exploring the roles of information in the control of vehicular locomotion: From kinematics and dynamics to cybernetics," *Presence: Teleoperators Virtual Environ.*, vol. 13, no. 5, pp. 535–548, 2004.

[7] O. Lappi and C. D. Mole, "Visuomotor control, eye movements, and steering: A unified approach for incorporating feedback, feedforward, and internal models," *Psychol. Bull.*, vol. 144, pp. 981–1001, 2018.

[8] J. P. Wann and M. F. Land, "Steering with or without the flow: Is the retrieval of heading necessary?" *Trends Cognitive Sci.*, vol. 4, no. 8, pp. 319–324, Aug. 2000.

[9] R. M. Wilkie and J. P. Wann, "Judgments of path, not heading, guide locomotion," *J. Exp. Psychol., Human Perception Perform.*, vol. 32, no. 1, pp. 88–96, 2006.

[10] C. D. Mole, G. Kountouriotis, J. Billington, and R. M. Wilkie, "Optic flow speed modulates guidance level control: New insights into two-level steering," *J. Exp. Psychol., Human Perception Perform.*, vol. 42, no. 11, pp. 1818–1838, Nov. 2016.

[11] M. F. Land and J. Horwood, "Which parts of the road guide steering?" *Nature*, vol. 377, pp. 339–340, Sep. 1995.

[12] P. M. van Leeuwen, R. Happee, and J. C. F. de Winter, "Vertical field of view restriction in driver training: A simulator-based evaluation," *Transp. Res. Part F*, vol. 24, pp. 169–182, May 2014.

[13] I. Frissen and F. Mars, "The effect of visual degradation on anticipatory and compensatory steering control," *Quart. J. Exp. Psychol.*, vol. 67, no. 3, pp. 499–507, 2014.

[14] M. F. Land and D. N. Lee, "Where we look when we steer," *Nature*, vol. 369, pp. 742–744, Jun. 1994.

[15] F. I. Kandil, A. Rotter, and M. Lappe, "Driving is smoother and more stable when using the tangent point," *J. Vis.*, vol. 9, pp. 1–11, 2009.

[16] O. Lappi, "Future path and tangent point models in the visual control of locomotion in curve driving," *J. Vis.*, vol. 14, no. 12, pp. 1–22, 2014.

[17] D. T. McRuer, R. W. Allen, D. H. Weir, and R. H. Klein, "New results in driver steering control models," *Human Factors*, vol. 19, no. 4, pp. 381–397, Aug. 1977.

[18] E. Donges, "A two-level model of driver steering behavior," *Human Factors*, vol. 20, no. 6, pp. 691–707, Dec. 1978.

[19] R. A. Hess and A. Modjtahedzadeh, "A control theoretic model of driver steering behavior," *IEEE Contr. Syst. Mag.*, vol. 10, no. 5, pp. 3–8, Aug. 1990.

[20] C. C. MacAdam, "Understanding and modeling the human driver," *Vehicle Syst. Dyn.*, vol. 40, no. 1–3, pp. 101–143, Jan. 2003.

[21] J. Steen, H. J. Damveld, R. Happee, M. M. van Paassen, and M. Mulder, "A review of visual driver models for system identification purposes," in *Proc. IEEE Int. Conf. Syst., Man, Cybern.*, 2011, pp. 2093–2100.

[22] D. D. Salvucci and R. Gray, "A two-point visual control model of steering," *Perception*, vol. 33, no. 10, pp. 1233–1248, Dec. 2004.

[23] C. Sentouh, P. Chevrel, F. Mars, and F. Claveau, "A sensorimotor driver model for steering control," in *Proc. IEEE Int. Conf. Syst., Man, Cybern.*, 2009, pp. 2462–2467.

[24] D. T. McRuer and H. R. Jex, "A review of quasi-linear pilot models," *IEEE Trans. Human Factors Electron.*, vol. HFE-8, no. 3, pp. 231–249, Sep. 1967.

[25] M. Mulder *et al.*, "Manual control cybernetics: State-of-the-art and current trends," *IEEE Trans. Human-Mach. Syst.*, vol. 48, no. 5, pp. 468–485, Oct. 2018.

[26] D. H. Weir and D. T. McRuer, "Measurement and interpretation of driver/vehicle system dynamic response," *Human Factors*, vol. 15, no. 4, pp. 367–378, 1973.

[27] A. J. Grunwald and S. J. Merhav, "Vehicular control by visual field cues-analytical model and experimental validation," *IEEE Trans. Syst., Man, Cybern.*, vol. SMCA-6, no. 12, pp. 835–845, Dec. 1976.

[28] B. T. Sweet, "The identification and modeling of visual cue usage in manual control task experiments," Ph.D. dissertation, Department of Aeronautics and Astronautics, Stanford University, Stanford, CA, USA, 1999.

[29] K. van der El, D. M. Pool, H. J. Damveld, M. M. van Paassen, and M. Mulder, "An empirical human controller model for preview tracking tasks," *IEEE Trans. Cybern.*, vol. 46, no. 11, pp. 2609–2621, Nov. 2016.

[30] K. van der El, S. Padmos, D. M. Pool, M. M. van Paassen, and M. Mulder, "Effects of preview time in manual tracking tasks," *IEEE Trans. Human-Mach. Syst.*, vol. 48, no. 5, pp. 486–495, Oct. 2018.

[31] K. van der El, D. M. Pool, M. M. van Paassen, and M. Mulder, "Identification and modeling of driver multiloop feedback and preview steering control," in *Proc. IEEE Int. Conf. Syst. Man Cybern.*, 2018, pp. 1227–1232.

[32] M. Mulder and J. A. Mulder, "Cybernetic analysis of perspective flight-path display dimensions," *J. Guid. Control Dyn.*, vol. 28, no. 3, pp. 398–411, 2005.

[33] L. Li and J. Chen, "Relative contributions of optic flow, bearing, and splay angle information to lane keeping," *J. Vis.*, vol. 10, no. 11, 2010.

[34] C. C. MacAdam, "Application of an optimal preview control for simulation of closed-loop automobile driving," *IEEE Trans. Syst., Man, Cybern.*, vol. SMCA-11, no. 6, pp. 393–399, Jun. 1981.

[35] E. R. Boer, "Tangent point oriented curve negotiation," in *Proc. IEEE Intell. Veh. Symp.*, Sep. 1996, pp. 7–12.

[36] R. L. Stapleford, D. T. McRuer, and R. E. Magdaleno, "Pilot describing function measurements in a multiloop task," *IEEE Trans. Human Factors Electron.*, vol. 8, no. 2, pp. 113–125, Jun. 1967.

[37] R. S. Sharp, D. Casanova, and P. Symonds, "A mathematical model for driver steering control, with design, tuning and performance results," *Veh. Syst. Dyn.*, vol. 33, no. 5, pp. 289–326, May 2000.

[38] D. T. McRuer and D. H. Weir, "Theory of manual vehicular control," *Ergonomics*, vol. 12, no. 4, pp. 599–633, 1969.

[39] R. A. Miller, "On the finite preview problem in manual control," *Int. J. Syst. Sci.*, vol. 7, no. 6, pp. 667–672, 1976.

[40] K. van der El, D. M. Pool, M. M. van Paassen, and M. Mulder, "Effects of preview on human control behavior in tracking tasks with various controlled elements," *IEEE Trans. Cybern.*, vol. 48, no. 4, pp. 1242–1252, Apr. 2018.

[41] E. Rezunenko, K. van der El, D. M. Pool, M. M. van Paassen, and M. Mulder, "Relating human gaze and manual control behavior in preview tracking tasks with spatial occlusion," in *Proc. IEEE Int. Conf. Syst., Man, Cybern.*, 2018, pp. 3440–3445.

[42] H. Zhao and W. H. Warren, "On-line and model-based approaches to the visual control of action," *Vis. Res.*, vol. 110, pp. 190–202, 2015.